https://doi.org/10.1595/205651323X16703459968311 *Johnson Matthey Technol. Rev.*, 2023, **67**, (1), 110–123

JOHNSON MATTHEY
TECHNOLOGY REVIEW

technology.matthey.com

Cathodes for Electrochemical Carbon Dioxide Reduction to Multi-Carbon Products: Part II

Rapid improvement in cathode performance

Harry Macpherson[$], Toby Hodges, Moyahabo Hellen Chuma
Johnson Matthey, Blounts Court, Sonning Common, Reading, RG4 9NH, UK

Connor Sherwin
University of Southampton, B29 Building, East Highfield Campus, University Road, SO17 1BJ, UK

Urša Podbevšek, Katie Rigg
Johnson Matthey, Blounts Court, Sonning Common, Reading, RG4 9NH, UK

Veronica Celorrio
Diamond Light Source, Harwell Science and Innovation Campus, Didcot, Oxfordshire, OX11 0DE, UK

Andrea Russell
University of Southampton, B29 Building, East Highfield Campus, University Road, SO17 1BJ, UK

Elena C. Corbos*
Johnson Matthey, Blounts Court, Sonning Common, Reading, RG4 9NH, UK

***Email:** crina.corbos@matthey.com

[$]Present address: Deep Science Ventures, 51 Eastcheap, 3rd Floor, London, EC3M 1JP, UK

PEER REVIEWED

Submitted 7th July 2022; Revised 26th October 2022; Accepted 27th October 2022; Online 31st October 2022

This is Part II of a focused review of recent highlights in the literature in cathode development for low temperature electrochemical carbon dioxide and carbon monoxide reduction to multi-carbon (C_{2+}) products. Part I (1) introduced the role of CO_2 reduction in decarbonising the chemical industry and described the catalysts and modelling approaches. Part II describes *in situ* characterisation to improve the understanding and development of catalysts, the catalyst layer and the gas diffusion layer.

1. *In Situ* Characterisation

1.1 Characterising Reaction Intermediates

Copper electrodes have been characterised through a range of different *in situ* and *operando* techniques to study the CO_2 reduction mechanism in real time. Prominent characterisation techniques include surface enhanced infrared adsorption spectroscopy (SEIRAS) and Raman spectroscopy which can both probe the surface intermediates during the reaction. Such characterisation can help improve the understanding and development of catalysts for improved C–C coupling.

The first step in the electrochemical CO_2 reduction reaction is the formation of the CO_2 radical anion ($*CO_2^-$), proposed by Hori *et al*. (2). This is the common intermediate between all reduction paths, beyond which formate or CO form. Chernyshova *et al.* (3) identified this intermediate through surface enhanced Raman spectroscopy (SERS) of a roughened copper electrode (**Table I**). They identified the first intermediate with the structure

Table I Table of Infrared and Raman Bands and their Assignments

Electrode	Electrolyte	Band Position, cm^{-1}	Infrared/ Raman	Assignment	Reference
Rough Cu	0.1 M $NaHCO_3$	2500–2070	Raman	C≡O Stretch of *CO	(3)
		280		Cu-CO frustrated rotation	
		360		Cu-CO translation	
		1065		$v_1CO_3^{2-}$ (symmetric C-O)	
		1540		$v_{as}CO_2^-$ (η^2(C,O)-CO^{2-})	
		350		vCu-C (η^2(C,O)-CO_2^-)	
Polycrystalline Cu	CO sat. 0.05 M Li_2CO_3	2000–2100	IR	C≡O Stretch (CO_{atop})	(4)
		1800–1900		C≡O Stretch (CO_{bridge})	
Cu(100)	CO sat. 0.1 M LiOH	1191	IR	C-O-H Stretch (OCCOH)	(5)
		1584		C-O Stretch (OCCOH)	
OD-Cu	CO sat. 0.05 M KOH	2058	IR	C≡O Stretch of *CO	(6)

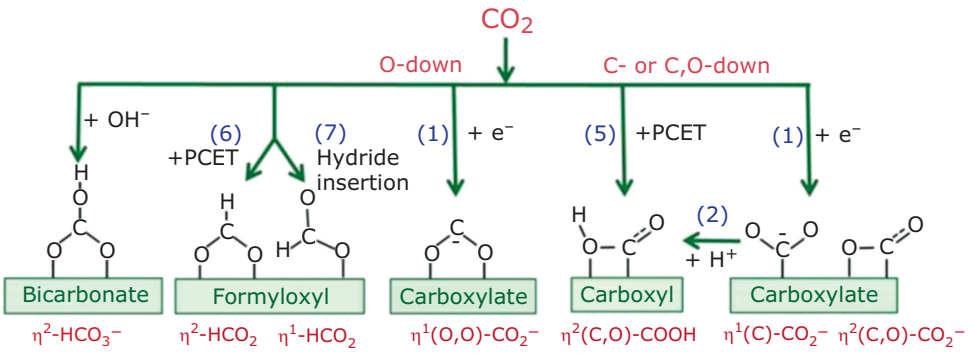

Fig. 1. Possible first intermediates of the CO_2 reduction reaction. Reprinted from (3)

η^2(C,O)-CO_2^- (**Figure 1**) which is stabilised onto the copper surface through the covalency of its two bonds to the copper surface, the charge polarisation of the system, the electrostatic interaction with the hydrated electrolyte cation and the positive charge of the coordinating copper atoms.

The adsorbed η^1(C)-CO_2^- or η^2(C,O)-CO_2^- can be converted to CO through protonation to form an adsorbed carboxyl and then reductively dissociates to CO and H_2O (2, 3), Equation (i) and (ii):

$$*CO_2^- + H^+ \rightarrow * COOH \quad \text{(i)}$$

$$*COOH + e^- + H^+ \rightarrow CO + H_2O \quad \text{(ii)}$$

CO is the important intermediate in the formation of C_{2+} products. Favourable adsorption of CO onto the copper surface promotes further reduction into C_{2+} products. The adsorption mode of CO onto the copper is also important, with a top-bound CO promoting further reduction whereas bridge-bound CO is less active (**Figure 2**) (4). The adsorption

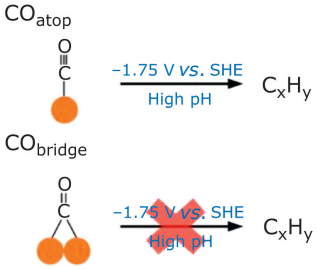

Fig. 2. Bonding modes of carbon monoxide onto copper surfaces. Reprinted with permission from (4), Copyright (2018) American Chemical Society

mode can be clearly distinguished from the infrared (IR) adsorption spectrum, with the bridge bound adsorption having an adsorption between 1800–1900 cm^{-1} and linearly bound between 2000–2100 cm^{-1} (**Table I**) (4).

Through *in situ* Fourier transform infrared of Cu(100) electrodes coupled with density functional theory calculations, stretching frequencies associated with C–O–H and C–O have

been identified during CO reduction. These were attributed to formation of the hydrogenated dimer OC–COH (**Table I**) (5). This provides evidence for C–C coupling taking place through a reductive dimerisation process early in the reaction. This process was however not found on Cu(111) electrodes under identical conditions, demonstrating the structure sensitivity of C–C coupling and its preference for square symmetry (6).

In contrast to metallic copper, electrodes prepared using copper oxides and derivates of copper oxide are favourable for producing C_{2+} products. Copper derived from Cu_2O has been shown to be highly selective towards C_{2+} products during CO reduction, with a 57% Faradaic efficiency (FE) at a modest potential of −0.3 V *vs*. reversible hydrogen electrode (RHE) in CO sat. 0.1 M KOH. *Operando* investigations of oxide-derived copper (OD-Cu) using attenuated total reflection SEIRAS (ATR-SEIRAS) have shown an adsorption band at 2058 cm^{-1} (7) similar to that of the linearly bound CO on Cu(100) (4). Thus, the ability of the oxide derived copper to facilitate C–C coupling at low overpotentials has been attributed to preferential exposure of the Cu(100) facet (7).

1.2 Probing Catalyst Changes

In situ techniques have also been used to determine the chemical and structural changes occurring at oxidised copper electrodes during the CO_2 reduction reaction. X-ray absorption spectroscopy (XAS) can determine bulk oxidation state changes, X-ray diffraction (XRD) spectroscopy provides information regarding changes to the crystal structure of the catalyst during the reaction, whilst Raman spectroscopy and X-ray photoelectron spectroscopy (XPS) can provide surface specific information.

According to the Pourbaix diagrams (8), in neutral electrolyte at CO_2 reduction reactions (CO_2RR) potentials copper should exist as copper metal. Therefore, over the course of CO_2RR a copper electrode typically reduces to metallic copper, a worse C_{2+} coupling catalyst than the oxides (9). Time dependent *in situ* Raman has been employed to look at the surface degradation of Cu_2O films during the CO_2RR. After holding the electrode at −0.99 V *vs*. RHE in CO_2 saturated $KHCO_3$, after 30 s the vibrations associated with Cu_2O were attenuated and two bands associated with intermediately reduced copper oxides appeared. After 200 s no peaks could be seen in the Raman spectrum suggesting it had been fully reduced to copper. Once the cathodic potential was removed, the surface re-oxidised to Cu_2O (10).

The Kauffman group (11) used *in situ* XAS, Raman spectroscopy and XRD to investigate the bulk and surface changes of porous copper oxides during CO_2 reduction (**Figure 3**). At open circuit potential the copper remains in the 2+ oxidation state however when a potential of −0.2 V *vs*. RHE is applied the presence of metallic copper is detected. At −0.6 V *vs*. RHE the material had almost completely reduced to Cu^0. This was also confirmed through *in situ* XRD, with the evolution of face-centred cubic copper when the potential was held at −0.6 V *vs*. RHE. However, once the cathodic potential was removed, the metallic copper was also found to re-oxidise. To investigate the surface changes and possible presence of surface oxides during the reaction (12–14), *in situ* Raman was also performed at −0.6 V *vs*. RHE. The A_g feature of CuO was monitored during the reaction, after 30 min this feature had completely gone, indicating the formation of Raman inactive metallic copper.

Copper oxide catalysts have been shown to reduce during the CO_2RR, but subsurface oxygen has been suggested as the reason for the improvement of oxide derived catalysts over metallic copper for C–C couplings (15). *In situ* ambient pressure XPS results has shown the absence of any residual oxide phases during CO_2RR, but did show the presence of subsurface oxygen (15, 16). Subsurface oxygen is believed to increase the CO binding energy through reduced sigma repulsion, favouring C–C bond formation through increased CO coverage (15).

Different methods of stabilising oxygenated copper species have been investigated. One promising example introduced nanocavities into the Cu_2O catalyst which confines the carbon intermediates formed *in situ* to remain in the cavity and cover the catalyst surface, stabilising the Cu^+ species. Through *in situ* Raman the characteristic Raman peaks for Cu_2O remained after 20 min at −0.61 V *vs*. RHE (**Figure 4**). Additional XAS of the catalysts during the 20 min cathodic hold shows 32.1% of the Cu^+ species remained after the potential hold (18).

De Luna *et al*. (19) have suggested 'electro re-deposited' copper catalyst made through partial dissolution of a copper precursor and redeposition of the copper ions as another catalyst capable of staying active for C_{2+} products for extended periods. They found this material has a C_{2+} FE of 52% at −1.2 V *vs*. RHE. *In situ* XAS during a potential hold at −1.2 V *vs*. RHE showed a reduction of the Cu^+ to metallic copper, from 84% Cu^+ at the start of

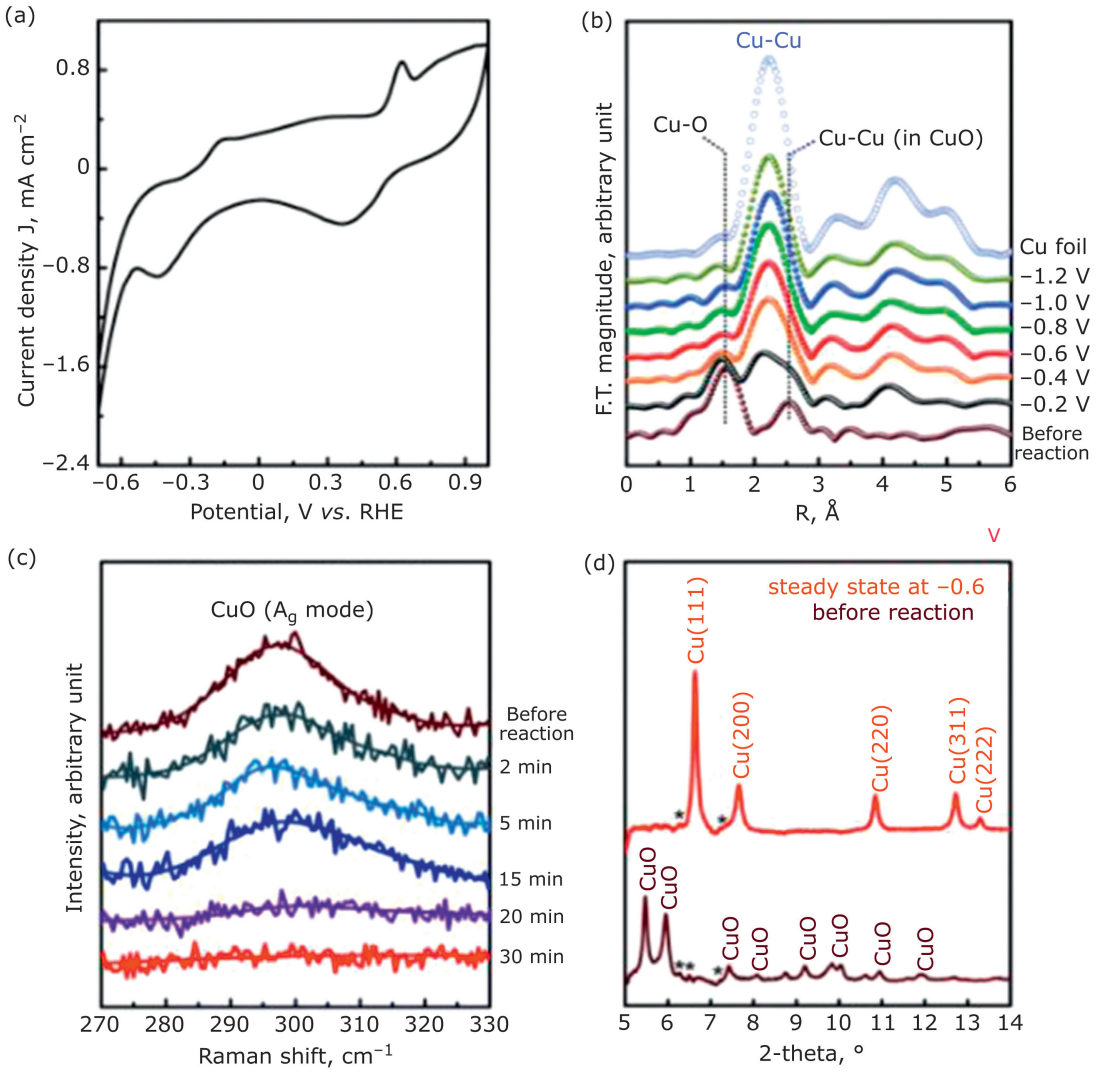

Fig. 3. (a) Cyclic voltammetry of CuO-IO electrode in CO_2 saturated 0.1 M $KHCO_3$; (b) potential-dependent k^2-weighted R-space extended X-ray absorption fine structure analysis (no phase correction) from −0.2 V to −1.2 V *vs*. RHE (collected at 30 min at each potential); (c) *in situ* Raman spectra for tracking surface structure of CuO-IO during EC-CO_2RR at −0.6 V (using 785 nm laser source); (d) single-crystal X-ray diffraction patterns of CuO-IO electrode under open circuit and steady state at −0.6 V *vs*. RHE. Used with permission of Royal Society of Chemistry from (11), Copyright (2019); permission conveyed through Copyright Clearance Center, Inc

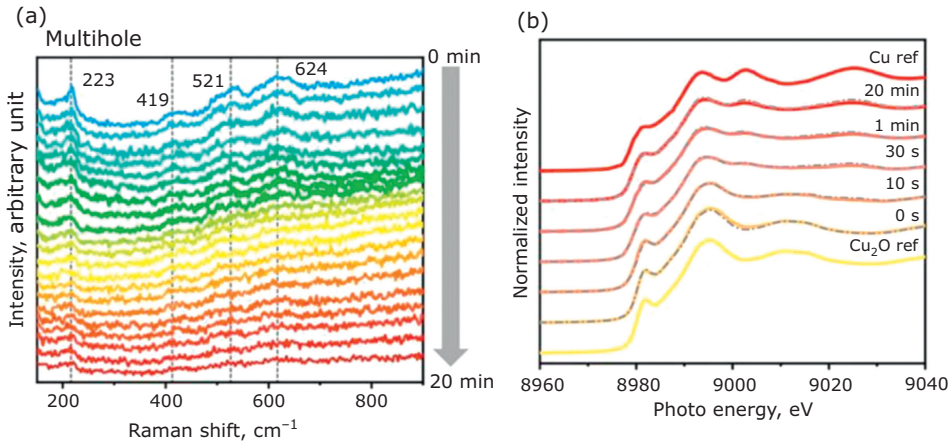

Fig. 4. (a) *Operando* Raman spectroscopy of Cu_2O during a potential hold of −0.61 V *vs*. RHE; (b) copper K-edge XAS spectra of Cu_2O at different times during a potential hold at −0.61 V *vs*. RHE. Reprinted with permission from (17), Copyright (2017) American Chemical Society

the reaction to 23% after 1 h. However, when a potential of –1.87 V *vs*. RHE was applied, the Cu^+ species was completely reduced to metallic copper.

In situ and *operando* techniques have been fundamental in understanding the electrochemical CO_2 reduction reaction mechanisms. SEIRAS and Raman spectroscopy have proven essential in characterising the initial intermediates forming during the reaction aiding in catalyst design to improve the selectivity and activity towards C_{2+} products. XAS, XRD, Raman spectroscopy and XPS have all been used to effectively show the changes occurring in the bulk and surface of the catalyst. This has helped understand the stability of copper oxides and how oxide derived copper catalysts can give higher selectivity towards carbon coupled products.

2. Catalyst Layer

The cathode catalyst layer (CL) must balance many competing demands and is one of the most crucial electrolyser components (20). Typically, it is a layer several hundred nanometres thick that at minimum comprises the catalyst, which is often in the form of nanoparticles. Polymers, especially ionomers, are commonly incorporated into the CL, primarily to provide mechanical stability and coherence by coating catalyst particles and adhering them to the substrate and each other. Polymers in the CL are therefore often called 'binders'. Polymers can, however, also be deposited in layers on top of the catalyst, and carbon nanoparticles are sometimes incorporated in the CL to improve electrical conductivity (21). The substrate onto which the CL is deposited depends on the electrolyser configuration. In a membrane-electrode assembly configuration akin to a polymer electrolyte water electrolyser, the CL may be directly deposited onto an ion exchange membrane. However, in the more commonly used configurations, in which electrolyte flows through a channel between the ion exchange membrane and the cathode, the CL is deposited onto a porous gas diffusion layer (GDL) and this configuration is the focus of this review. CL deposition is commonly achieved by producing an ink, containing binder and catalyst, which is deposited onto the GDL by spray coating, calendaring, drop casting, hot pressing or bar coating. The method of coating affects reproducibility and product selectivity, with more controllable methods such as automatic spray coating producing more consistent and homogeneous layers (20). A different possible approach involves directly coating the catalyst to the GDL by sputtering or physical or chemical vapour deposition.

The number one priority in CL design in CO_2 electrolysis to C_{2+} products is high FE for such products. Achieving this not only requires high activities (i.e. high partial current densities) for C_{2+} products but also the suppression of the parasitic hydrogen evolution reaction (HER) and pathways to C1 products. Looking at **Table II**, CO_2RR require CO_2 and protons, in contrast to HER. Therefore, sufficient mass transport of CO_2 to the electrocatalyst surface is required to kinetically favour CO_2RR. To maintain sufficient CO_2 transport, it is essential the CL does not become fully wetted or 'flooded' with electrolyte, and this is a leading cause of cell failure.

A high local pH at the catalyst surface also promotes C_{2+} products by suppressing pathways to C1 products for which proton transfer is the rate limiting step.

Therefore, CLs should ideally be engineered for maximum transport of CO_2 but relatively slow transport of OH^- produced in the cathode reactions and buffering ions such as HCO_3^- from the bulk electrolyte.

An important function of the CL is to maintain triple phase boundaries where CO_2, protons and electrons can meet. This is challenging because liquid transport is enhanced by hydrophilicity, yet this hinders gas transport, and furthermore hydrophobic materials tend not to be electrically conductive. Therefore, the design of active and selective CLs involves an optimisation of competing material properties.

Table II The Electrochemical Half Equations of CO_2 to Commonly Reported Products, with their Associated Reduction Potentials *vs*. Standard Hydrogen Electrode (22)

Half-cell reaction	Potential *vs*. standard hydrogen electrode
$CO_{2(g)} + 2H^+ + 2e^- \leftrightarrow CO_{(g)} + H_2O_{(l)}$	–0.106
$2CO_{2(g)} + 12H^+ + 12e^- \leftrightarrow C_2H_{4(g)} + 4H_2O_{(l)}$	0.064
$2H^+ + 2e^- \leftrightarrow H_{2(g)}$	0.000

Maintaining sufficient hydrophobicity in long term operation is made challenging by several phenomena. First, electrowetting of copper CL's can occur merely as a result of the application of potential (23). Second, liquid products such as formic acid and alcohols decrease surface tension of the electrolyte and can cause flooding at high concentrations (24). Third, the precipitation of hydrophilic solid carbonates and bicarbonates in the CL can also cause flooding and block gas transport (25). A common strategy to mitigate flooding and reduce selectivity for HER is to increase the hydrophobicity of the CL and this is often achieved by incorporating binders such as polytetrafluoroethylene (PTFE). However, the addition of too much PTFE can significantly reduce the conductivity of the CL (26). A 2022 study (27) compared coatings onto copper nanoneedles of polyacrylic acid (PAA), which is hydrophilic; Nafion®, which contains hydrophilic and hydrophobic domains; and fluorinated ethylene propylene (FEP), which is totally hydrophobic and is similar to PTFE in structure.

As shown in **Figure 5(a)**, the contact angle of the electrolyte with the CL was highest for the electrode incorporating FEP, followed by Nafion® and PAA, confirming that the more hydrophobic the binder the more hydrophobic the CL. Using the captive bubble contact angle method, the CO_2-phillicity was determined to be highest for the FEP electrode, followed by Nafion® and PAA, confirming that gas accessibility increases with hydrophobicity. Potentiostatic electrolysis was then conducted in a flow cell using GDEs with CLs incorporating the three polymers. As detailed in **Figure 5(b)**, the more hydrophobic the CL, the greater the FE for CO_2RR products and the lower the FE for HER, and furthermore the higher the FE for C_{2+} products. The improved selectivity for CO_2RR products is explained by increased concentration of CO_2 relative to H_2O at the catalyst surface, due to the microhydrophobic environment in the vicinity of the binder, which increases CO_2 gas access while limiting H_2O access, as illustrated in **Figure 5(c)** and **5(d)**. It was further posited that the improved selectivity to C_{2+} products was a result of improved

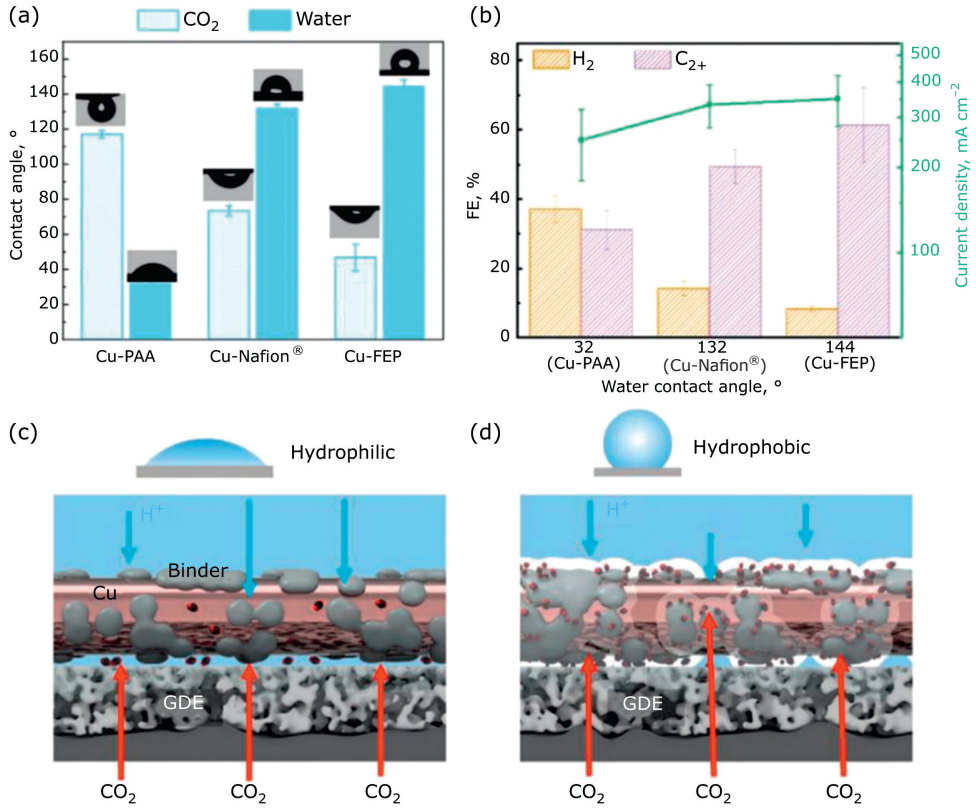

Fig. 5. (a) Water and CO_2 contact angles for CLs prepared with PAA, Nafion® and FEP; (b) total current density and FEs for H_2 and C_{2+} products as a function of the hydrophilicity, acquired in flow cell at –0.71 V *vs*. RHE, with aqueous 1.0 m KOH as electrolyte; (c) hydrophilic and (d) hydrophobic schematic illustrations of the local reaction environment near the copper surface in a flow cell. Reprinted from (27) under a Creative Commons Attribution-NonCommercial License

accessibility of CO at the catalyst surface which further reacts to C_{2+} compounds.

Other recent studies have improved CO_2RR selectivity by employing hydrophobic binders in the CL (28–30). Kim *et al.* (31) measured the water concentration on thin ionomer films deposited onto bare metallic copper, finding that both Nafion® and Sustainion®, a hydrocarbon anion exchange ionomer, reduced water concentration compared to bare copper. Nafion®, with its very hydrophobic perfluorinated backbone, had a lower water concentration than Sustainion®, and Nafion® with an equivalent weight of 1100, denoted 'Naf1100' in **Figure 6**, had a lower concentration than Naf850, which has a higher density of hydrophilic sulfonate groups. This highlights the prospect of varying the equivalent weight of ionomers to modulate hydrophobicity.

An area which has so far received little attention is the influence of ink composition on hydrophobicity and more generally CL performance. Although the ink solvent is evaporated following, or even during, CL deposition and so does not remain in the CL, it can still have a profound effect on the CL structure. A 2021 study (32) produced inks of a silver catalyst with Aemion CNN-8 anion exchange ionomer using methanol, ethanol and different ratios of water and isopropanol, finding the ink solvent to have a large influence on CL properties and that the CLs exhibiting the highest hydrophobicity and capillarity had the highest FEs for CO_2RR. It was also found that an intermediate level of ionomer aggregation was beneficial for CO_2RR as this facilitated the formation of ionomer-catalyst aggregates. Too little aggregation resulted in the formation of a less porous CL, whereas too much resulted in regions of concentrated ionomer and exposed catalyst.

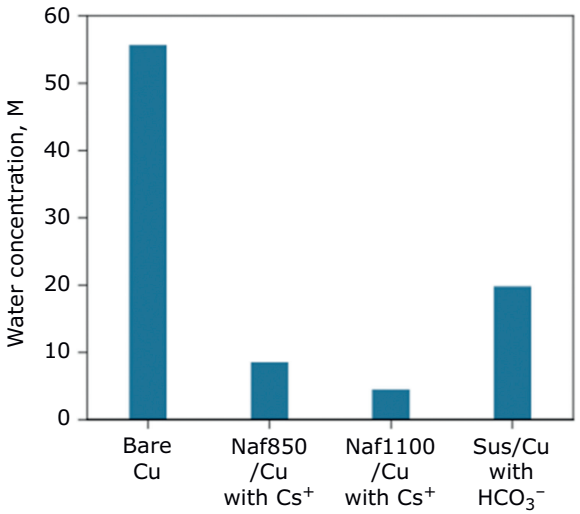

Fig. 6. Measurement of water concentration for ionomer-coated copper at 100% relative humidity; each sample was ion-exchanged using 0.1 M $CsHCO_3$ solution before the measurement. Reprinted from (31), Copyright (2021) Springer Nature

Several parameters in CL design affect local pH, one of the simplest being the thickness of the CL, which can be controlled by varying the catalyst loading. A 2021 study (33) found that high catalyst loadings of around 1.0 mg cm^{-2} increased ethylene selectivity because the thicker CLs act as a barrier for mass transport of buffering HCO_3^- ions that were present in the electrolyte, thereby increasing local pH in the region of the CL closest to the microporous layer (MPL) of the GDL. Similarly, thick CLs can also increase local pH by inhibiting transport of OH^- produced at the cathode (34). Contrariwise, in concentrated alkaline electrolytes, such as 10 M KOH, C_{2+} selectivity is enhanced by employing CLs as thin as 25 nm (21). This is because in such alkaline electrolytes, CO_2 is unable to penetrate far into the CL before being consumed by reaction with OH^-, meaning regions of the CL furthest from the MPL receive insufficient mass transport of CO_2. However, the rapid consumption of the electrolyte in highly alkaline cells has been recognised as a serious problem for overall energy consumption in recent years, making cells using near-neutral electrolyte more relevant to study (35). In near-neutral buffering electrolytes, high Nafion® loading can also enhance C_{2+} selectivity by further slowing transport of HCO_3^- ions, however increasing the loading to 50 wt% reduces selectivity by limiting transport of CO_2. Cation exchange ionomers such as Nafion® are proposed to slow transport of OH^- and HCO_3^- *via* Donnan exclusion (31, 36).

Taking a different approach to increasing local pH, a 2021 paper (37) reported the production of GDEs by co-electrodeposition of copper and polyamines, as shown schematically in **Figure 7**. Polymers with various degrees of amine functionalisation were deposited from solution along with copper, such that the amines were adhered to the surface of the deposited copper particles. The polymers with the highest density of amine groups were found to give the highest current density and FE for ethylene when tested in an alkaline flow cell, and this was rationalised by their ability to increase pH at the catalyst surface by setting up the following acid-base equilibrium, Equation (iii):

$$HCO_3^- + R\text{-}NH_2 \leftrightarrow CO_3^{2-} + R\text{-}NH_3^+ \quad \text{(iii)}$$

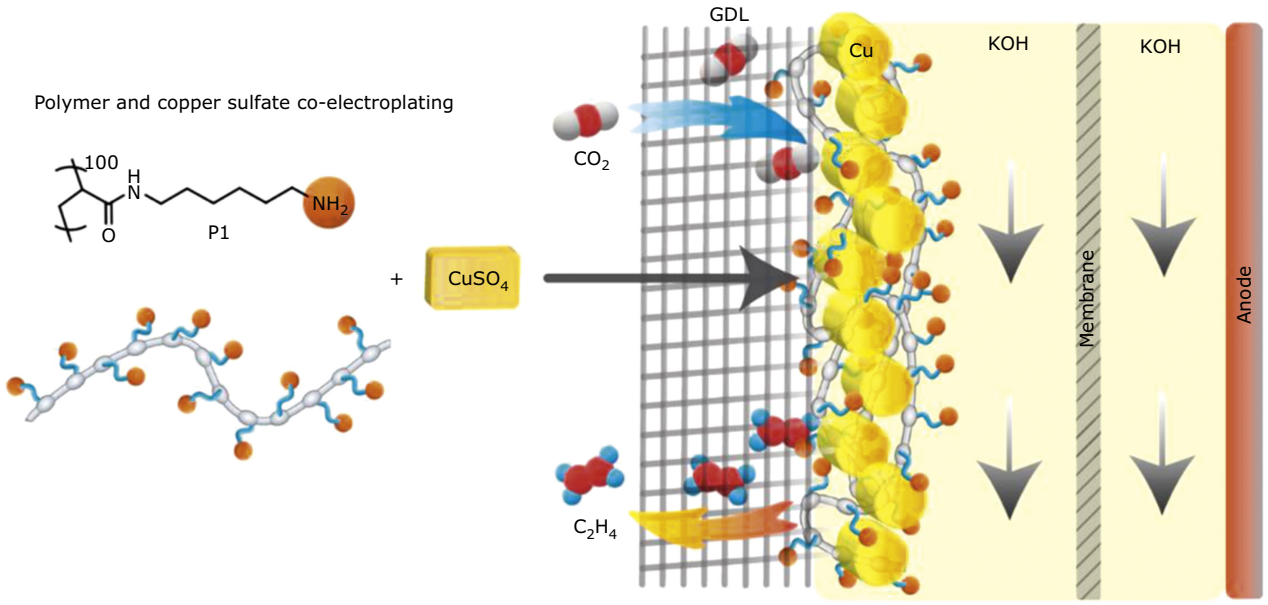

Fig. 7. Schematic illustration of co-electrodeposition of copper and polyamine to a GDL

The presence of amine groups shifts the equilibrium to the right towards greater CO_3^{2-} concentration and therefore higher surface pH. The increase in ethylene selectivity may however also have been due to an increase in surface CO concentration facilitated by the polymer aiding C–C coupling.

A less discussed parameter affecting local CO_2 concentration at the catalyst surface is the solubility of CO_2 in the binder. For example, the solubility of CO_2 in Sustainion® is 20 times higher than in Nafion® (31) due to its imidazolium functional groups (38). As shown in **Figure 8**, increasing the CO_2 concentration in the CL and, in particular, increasing the ratio of CO_2 to water, increases the partial current density for CO_2 reduction.

For significant progress to be made in sustaining high selectivity, an innovation in the CL will be required which allows it to break out of the current compromise between gas transport, electrolyte species transport and conductivity. One proposal (39) for how to do this is to de-couple hydroxide, CO_2 and water transport by making use of binders with separate hydrophilic and hydrophobic domains and potentially by bringing polyfluorosulfonic acid and anion exchange ionomers into close contact with the catalyst.

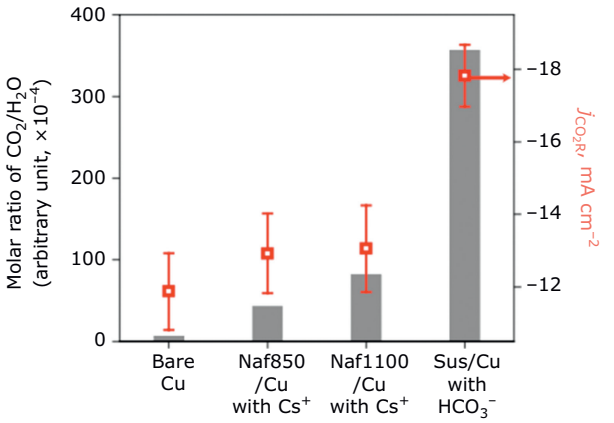

Fig. 8. Estimation of local CO_2:H_2O on the basis of measured water concentration and corresponding partial current densities at –1.15 V *vs*. RHE in 0.1 M $CsHCO_3$. Reprinted from (31), Copyright (2021) Springer Nature

3. Gas Diffusion Layer

The GDL serves as a mechanical support to the CL to form a GDE. Crucially, the GDL provides a pathway for CO_2 gas to reach the CL and thus enables an order of magnitude higher CO_2RR current densities (hundreds of mA cm^{-2}) than when gas is fed to the electrode through dissolution and diffusion in bulk electrolyte (tens of mA cm^{-2}) (40, 41). At the same time, the catalyst must be in direct contact with a liquid or solid electrolyte that provides protons and sustains ionic current conduction. The GDE must also sustain electrical contact without significant ohmic loses, either by using an inherently conductive GDL, such as carbon paper, or by containing an additional conductive layer (21).

Since it defines the rate of mass transport to and from the CL, a GDL has a defining role to play in tuning the selectivity of the conversion by defining the concentration of reactants and products in the local catalyst environment. Intentional design of GDL structures and compositions that would provide favourable conditions for selectively producing a desired product has been identified as an important challenge in the development of economically feasible electrolysers yet is not well understood (39–41).

In addition to selectivity tuning, the GDL must also provide sufficient resistance to flooding by simultaneously allowing the presence of water as a proton source in the CL while preventing detrimental permeation of water and liquid products into the layer.

3.1 Selectivity Studies by Model Electrodes

To guide GDE design towards improving selectivity for C_{2+} products, well-defined structures made of copper have been designed and studied (42, 43). Well-defined geometries of such model electrodes enable insight into the complex interplay between the mass transport and local chemical environment. They offer a rationalised context to the many experimental observations reporting sensitivity of the CO_2RR selectivity to the structure of the GDE (41). Pérez-Ramírez *et al.* designed a microstructure electrode using laser ablation to define uniform and evenly distributed conical cavities in a copper foil (**Figure 9(a)**) (43). The well-defined and tuneable micrometre-scale geometry enabled quantitative description of the local chemical environment established inside the cavities during the CO_2RR reaction. By combining experimental current densities and FEs with the descriptors of the chemical environment inside the pores (average local CO_2 concentration and pH), they were able to map selectivity towards selected products versus the local conditions. These descriptors are well-known to strongly influence the selectivity of CO_2 reduction (44, 45), however accurately quantifying their contribution has remained elusive.

Figure 9(b) shows a visualisation of the sensitivity of reaction selectivity on the local conditions. The overlap of ethylene and ethanol production peaks suggests it may not be possible to discriminate between these two products by

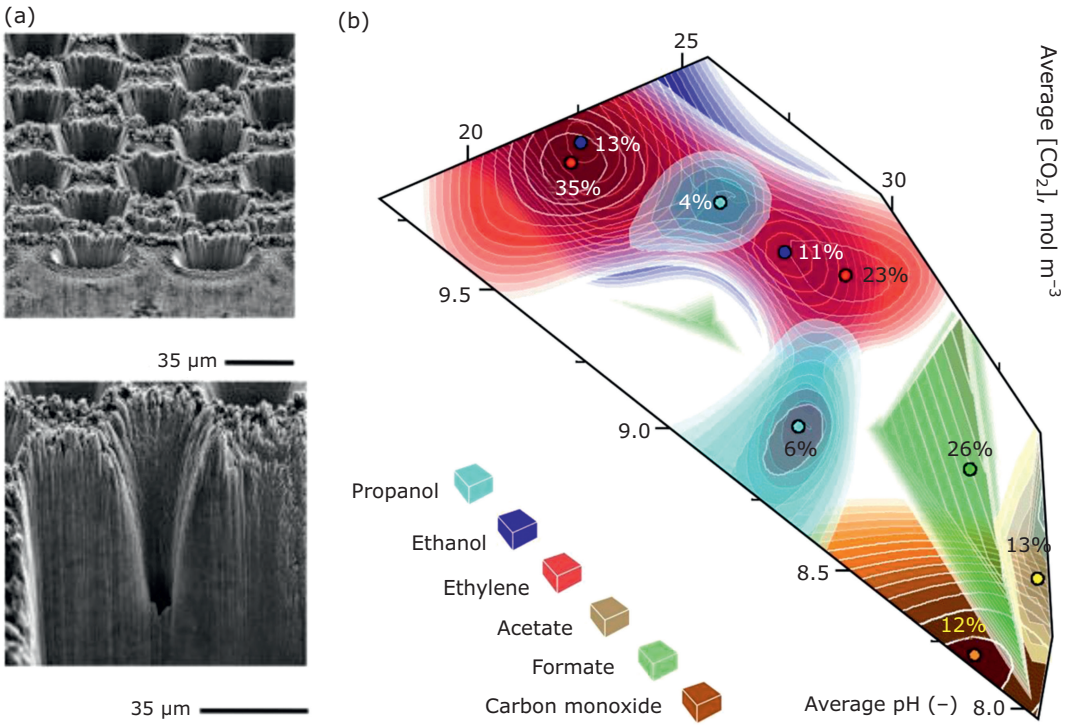

Fig. 9. (a) Scanning electron micrographs of the surface and cross-section of the laser-etched copper foil with conical cavities; (b) overlaid selectivity maps plotting the FE towards selected CO_2RR in relation to average pH and CO_2 concentration as descriptors. Reprinted from (43), Copyright (2020), with permission from Elsevier

tuning the local conditions. Another insight can be gained by analysing the two FE peaks for propanol, which suggest two different reaction pathways may be favoured at different local conditions. The intermediate pH and high CO_2 concentration are hypothesised to offer the optimal balance between C_1 and C_2 production, leading to C_3 products.

As well as model electrodes, practical GDLs can also be manufactured with well-defined and controlled structural parameters such as pore size and shape. A three-dimensional (3D) printable GDL has been developed with tuneable microporous structure of a fluoropolymer-based GDL, which allowed CO_2 permeance through the GDL to be modulated over several orders of magnitude (46). By tuning the structural parameters, an optimised GDL structure was obtained that allowed the FE towards ethylene to be maximised at high current densities. The authors suggested prolonging the residence time of the CO intermediate near the catalyst, achieved with the optimised GDL design, as the main reason for improved performance.

3.2 Composition for Flooding Prevention

While using GDL enables high current densities and allows the conversion selectivity to be modulated, the most pertinent challenge that still requires a breakthrough remains water management (47, 48). Flooding is the key issue preventing electrolyser operation for relevant times (24). Even the currently best-performing systems, which sustain stable operation for over 100 h (21) are still far away from the durability that will eventually be required in practical CO_2 electrolysers (>5000 h) (49).

Flooding is governed by surface properties of the GDE components. Most commonly the wettability is managed by the GDL by either using hydrophobic materials such as fluorinated polymers as coatings for the surface of otherwise hydrophilic carbon (50), or as the main GDL component (21, 46). Preventing flooding failure through micro-structuring (optimising pore geometry, size distribution and connectivity) has also been suggested (24, 51).

Polymer-coated carbon-based GDLs have been reported to enable C_{2+} products with comparatively high FEs (21). The initial hydrophobicity, however, is lost within a few hours under high-current density operation conditions, which leads to flooding. It has been suggested that this is due to the applied potential (50) and degradation of the coating, accelerated under the locally alkaline conditions (47, 50). Another downside of using carbon as the GDL material is that it can catalyse the HER, which decreases the FE towards carbon products (50).

Significantly longer operational times (>100 h) at high current density have been achieved when the carbon GDL was replaced by an expanded PTFE membrane (21). What is more, the selectivity towards C_{2+} product at relevant current densities (>100 mA cm^{-2}) was improved (21, 52). To introduce sufficient electron conductivity, a layer of sputtered copper catalyst has been additionally coated with a layer of carbon black particles and graphite (21).

The desired improvement in production rates, FEs and durability can, however, make flooding prevention even more challenging by accumulating liquid C_{2+} products that lower the surface tension of the electrolyte, such as ethanol and 1-propanol. Although concentrating the products in the electrolyser outlet is highly desired from a technoeconomic point of view, producing such mixtures can be detrimental even to the currently top-performing hydrophobic fluoropolymer-based GDLs, as demonstrated by Leonard *et al.* (24) for water-alcohol mixtures on PTFE surface. They suggested introducing additional surface treatments to the hydrophobic fluoropolymer-based GDLs in order to make them oleophobic and resistant to wetting of product-rich outlets.

In a recent report, Lapkin *et al.* present a case for deposition of a hydrophilic residue on the electrode surface while producing ethylene on copper (53). They proposed that acrolein, an unsaturated C_3 aldehyde not previously reported as a CO_2RR product on copper, was formed during the reaction in low concentrations. Under the locally alkaline conditions at the catalyst surface, acrolein was hypothesised to polymerise into hydrophilic oligomers and polymers that were found deposited on the electrode surface in post-mortem analysis. Acrolein thus avoided direct *operando* detection, but nevertheless promoted flooding by making the catalyst surface hydrophilic.

The pressing challenge for CO_2RR to C_{2+} products is designing a GDL that will provide wetting-resistant functionalities for extended run times in the presence of concentrated products. Additionally, the mass-controlling function of the GDL can in combination with the design of the CL modulate the selectivity of the overall conversion by careful tuning of the local conditions that facilitate formation of the selected C_{2+} product(s). There is

growing need to expand our understanding of this complex but relevant effects (46).

4. Conclusions

While the rate of improvement in cathode performance has been rapid in recent years, achieving prolonged product selectivity will require both greater understanding and ingenuity. Not only must the cathode components be optimised in their own right, but their interactions must be understood and harnessed. While this complexity and interdependence makes establishing solid facts challenging, the potent combination of standard electrochemical testing with *in situ* characterisation and modelling will likely continue to be instrumental in advancing the field.

Authors Contributions

Harry Macpherson wrote the 'Catalyst Layer' section and created the layout of the review; Toby Hodges wrote the 'Catalysts' section; Moyahabo H. Chuma wrote the 'Modelling' section; Connor Sherwin wrote the '*In Situ* Characterisation' section; Urša Podbevšek wrote the 'Gas Diffusion Layer' section; Katie Rigg, Veronica Celorrio and Andrea Russell contributed to the '*In Situ* Characterisation' section; Elena C. Corbos proofread the manuscript and gave overall advice.

Acknowledgements

We acknowledge European Commission Horizon 2020 research and innovation program for funding Renewable Electricity-based, Cyclic and Economic Production of Fuel (EcoFuel) project under grant agreement 101006701 and Heterogenous Photo(electro)catalysis in Flow using Concentrated Light: modular integrated designs for the production of useful chemicals (FlowPhotoChem) under grant agreement No 862453. The material presented and views expressed here are the responsibility of the authors only. The EU Commission takes no responsibility for any use made of the information set out.

Connor Sherwin would like to acknowledge Chris Zalitis (Johnson Matthey, UK) for his support and guidance, and fruitful discussions.

References

1. H. Macpherson, T. Hodges, M. H. Chuma, C. Sherwin, U. Podbevšek, K. Rigg, V. Celorrio, A. Russell and E. C. Corbos, *Johnson Matthey Technol. Rev.*, 2023, **67**, (1), 97
2. Y. Hori, 'Electrochemical CO_2 Reduction on Metal Electrodes', in "Modern Aspects of Electrochemistry 42", eds. C. G. Vayenas, R. E. White and M. E. Gamboa-Aldeco, Ch. 3, Springer-Verlag, New York, USA, 2008, pp. 89–189
3. I. V. Chernyshova, P. Somasundaran and S. Ponnurangam, *Proc. Natl. Acad. Sci. USA*, 2018, **115**, (40), E9261
4. C. M. Gunathunge, V. J. Ovalle, Y. Li, M. J. Janik and M. M. Waegele, *ACS Catal.*, 2018, **8**, (8), 7507
5. E. Pérez-Gallent, M. C. Figueiredo, F. Calle-Vallejo and M. T. M. Koper, *Angew. Chem. Int. Ed.*, 2017, **56**, (13), 3621
6. K. J. P. Schouten, E. Pérez Gallent and M. T. M. Koper, *ACS Catal.*, 2013, **3**, (6), 1292
7. A. S. Malkani, M. Dunwell and B. Xu, *ACS Catal.*, 2019, **9**, (1), 474
8. B. Beverskog and I. Puigdomenech, *J. Electrochem. Soc.*, 1997, **144**, (10), 3476
9. S. Nitopi, E. Bertheussen, S. B. Scott, X. Liu, A. K. Engstfeld, S. Horch, B. Seger, I. E. L. Stephens, K. Chan, C. Hahn, J. K. Nørskov, T. F. Jaramillo and I. Chorkendorff, *Chem. Rev.*, 2019, **119**, (12), 7610
10. D. Ren, Y. Deng, A. D. Handoko, C. S. Chen, S. Malkhandi and B. S. Yeo, *ACS Catal.*, 2015, **5**, (5), 2814
11. T.-D. Nguyen-Phan, C. Wang, C. M. Marin, Y. Zhou, E. Stavitski, E. J. Popczun, Y. Yu, W. Xu, B. H. Howard, M. Y. Stuckman, I. Waluyo, P. R. Ohodnicki and D. R. Kauffman, *J. Mater. Chem. A*, 2019, **7**, (48), 27576
12. L. Mandal, K. R. Yang, M. R. Motapothula, D. Ren, P. Lobaccaro, A. Patra, M. Sherburne, V. S. Batista, B. S. Yeo, J. W. Ager, J. Martin and T. Venkatesan, *ACS Appl. Mater. Interfaces*, 2018, **10**, (10), 8574
13. H. Mistry, A. S. Varela, C. S. Bonifacio, I. Zegkinoglou, I. Sinev, Y.-W. Choi, K. Kisslinger, E. A. Stach, J. C. Yang, P. Strasser and B. R. Cuenya, *Nat. Commun.*, 2016, **7**, 12123
14. A. Eilert, F. S. Roberts, D. Friebel and A. Nilsson, *J. Phys. Chem. Lett.*, 2016, **7**, (8), 1466
15. A. Eilert, F. Cavalca, F. S. Roberts, J. Osterwalder, C. Liu, M. Favaro, E. J. Crumlin, H. Ogasawara, D. Friebel, L. G. M. Pettersson and A. Nilsson, *J. Phys. Chem. Lett.*, 2017, **8**, (1), 285,
16. D. Gao, I. Zegkinoglou, N. J. Divins, F. Scholten, I. Sinev, P. Grosse and B. Roldan Cuenya, *ACS Nano*, 2017, **11**, (5), 4825
17. S. Ma, M. Sadakiyo, M. Heima, R. Luo, R. T. Haasch, J. I. Gold, M. Yamauchi and P. J. A. Kenis, *J. Am. Chem. Soc.*, 2017, **139**, (1), 47

18. P.-P. Yang, X.-L. Zhang, F.-Y. Gao, Y.-R. Zheng, Z.-Z. Niu, X. Yu, R. Liu, Z.-Z. Wu, S. Qin, L.-P. Chi, Y. Duan, T. Ma, X.-S. Zheng, J.-F. Zhu, H.-J. Wang, M.-R. Gao and S.-H. Yu, *J. Am. Chem. Soc.*, 2020, **142**, (13), 6400
19. P. De Luna, R. Quintero-Bermudez, C.-T. Dinh, M. B. Ross, O. S. Bushuyev, P. Todorović, T. Regier, S. O. Kelley, P. Yang and E. H. Sargent, *Nat. Catal.*, 2018, **1**, (2), 103
20. H.-R. "M." Jhong, F. R. Brushett and P. J. A. Kenis, *Adv. Energy Mater.*, 2013, **3**, (5), 589
21. C.-T. Dinh, T. Burdyny, M. G. Kibria, A. Seifitokaldani, C. M. Gabardo, F. P. García de Arquer, A. Kiani, J. P. Edwards, P. De Luna, O. S. Bushuyev, C. Zou, R. Quintero-Bermudez, Y. Pang, D. Sinton and E. H. Sargent, *Science*, 2018, **360**, (6390), 783
22. M. Jouny, W. Luc and F. Jiao, *Ind. Eng. Chem. Res.*, 2018, **57**, (6), 2165
23. K. Liu, W. A. Smith and T. Burdyny, *ACS Energy Lett.*, 2019, **4**, (3), 639
24. M. E. Leonard, M. J. Orella, N. Aiello, Y. Román-Leshkov, A. Forner-Cuenca and F. R. Brushett, *J. Electrochem. Soc.*, 2020, **167**, (12), 124521
25. D. G. Wheeler, B. A. W. Mowbray, A. Reyes, F. Habibzadeh, J. He and C. P. Berlinguette, *Energy Environ. Sci.*, 2020, **13**, (12), 5126
26. K. J. Puring, D. Siegmund, J. Timm, F. Möllenbruck, S. Schemme, R. Marschall and U.-P. Apfel, *Adv. Sustain. Syst.*, 2021, **5**, (1), 2000088
27. T. H. M. Pham, J. Zhang, M. Li, T.-H. Shen, Y. Ko, V. Tileli, W. Luo and A. Züttel, *Adv. Energy Mater.*, 2022, **12**, (9), 2103663
28. P. An, L. Wei, H. Li, B. Yang, K. Liu, J. Fu, H. Li, H. Liu, J. Hu, Y.-R. Lu, H. Pan, T.-S. Chan, N. Zhang and M. Liu, *J. Mater. Chem. A*, 2020, **8**, (31), 15936
29. M. Wang, L. Wan and J. Luo, *Nanoscale*, 2021, **13**, (6), 3588
30. Q. Chang, J. H. Lee, Y. Liu, Z. Xie, S. Hwang, N. S. Marinkovic, A.-H. A. Park, S. Kattel and J. G. Chen, *JACS Au*, 2021, **2**, (1), 214
31. C. Kim, J. C. Bui, X. Luo, J. K. Cooper, A. Kusoglu, A. Z. Weber and A. T. Bell, *Nat. Energy*, 2021, **6**, (11), 1026
32. B. A. W. Mowbray, D. J. Dvorak, N. Taherimakhsousi and C. P. Berlinguette, *Energy Fuels*, 2021, **35**, (23), 19178
33. T. Möller, T. N. Thanh, X. Wang, W. Ju, Z. Jovanov and P. Strasser, *Energy Environ. Sci.*, 2021, **14**, (11), 5995
34. S. Suter and S. Haussener, *Energy Environ. Sci.*, 2019, **12**, (5), 1668
35. J. Sisler, S. Khan, A. H. Ip, M. W. Schreiber, S. A. Jaffer, E. R. Bobicki, C.-T. Dinh and E. H. Sargent, *ACS Energy Lett.*, 2021, **6**, (3), 997
36. D. A. Vermaas, S. Wiegman, T. Nagaki and W. A. Smith, *Sustain. Energy Fuels*, 2018, **2**, (9), 2006
37. X. Chen, J. Chen, N. M. Alghoraibi, D. A. Henckel, R. Zhang, U. O. Nwabara, K. E. Madsen, P. J. A. Kenis, S. C. Zimmerman and A. A. Gewirth, *Nat. Catal.*, 2021, **4**, (1), 20
38. S. Zulfiqar, M. I. Sarwar and D. Mecerreyes, *Polym. Chem.*, 2015, **6**, (36), 6435
39. E. W. Lees, B. A. W. Mowbray, F. G. L. Parlane and C. P. Berlinguette, *Nat. Rev. Mater.*, 2022, **7**, (1), 55
40. D. Wakerley, S. Lamaison, J. Wicks, A. Clemens, J. Feaster, D. Corral, S. A. Jaffer, A. Sarkar, M. Fontecave, E. B. Duoss, S. Baker, E. H. Sargent, T. F. Jaramillo and C. Hahn, *Nat. Energy*, 2022, **7**, (2), 130
41. D. Higgins, C. Hahn, C. Xiang, T. F. Jaramillo and A. Z. Weber, *ACS Energy Lett.*, 2019, **4**, (1), 317
42. K. D. Yang, W. R. Ko, J. H. Lee, S. J. Kim, H. Lee, M. H. Lee and K. T. Nam, *Angew. Chem. Int. Ed.*, 2017, **56**, (3), 796
43. F. L. P. Veenstra, N. Ackerl, A. J. Martín and J. Pérez-Ramírez, *Chem*, 2020, **6**, (7), 1707
44. Y. C. Tan, K. B. Lee, H. Song and J. Oh, *Joule*, 2020, **4**, (5), 1104
45. A. S. Varela, *Curr. Opin. Green Sustain. Chem.*, 2020, **26**, 100371
46. J. Wicks, M. L. Jue, V. A. Beck, J. S. Oakdale, N. A. Dudukovic, A. L. Clemens, S. Liang, M. E. Ellis, G. Lee, S. E. Baker, E. B. Duoss and E. H. Sargent, *Adv. Mater.*, 2021, **33**, (7), 2003855
47. M. E. Leonard, L. E. Clarke, A. Forner-Cuenca, S. M. Brown and F. R. Brushett, *ChemSusChem*, 2020, **13**, (2), 400
48. M. Li, M. N. Idros, Y. Wu, T. Burdyny, S. Garg, X. S. Zhao, G. Wang and T. E. Rufford, *J. Mater. Chem. A*, 2021, **9**, (35), 19369
49. A. J. Martín, G. O. Larrazábal and J. Pérez-Ramírez, *Green Chem.*, 2015, **17**, (12), 5114
50. K. Yang, R. Kas, W. A. Smith and T. Burdyny, *ACS Energy Lett.*, 2021, **6**, (1), 33
51. Z.-Z. Niu, F.-Y. Gao, X.-L. Zhang, P.-P. Yang, R. Liu, L.-P. Chi, Z.-Z. Wu, S. Qin, X. Yu and M.-R. Gao, *J. Am. Chem. Soc.*, 2021, **143**, (21), 8011
52. C. M. Gabardo, C. P. O'Brien, J. P. Edwards, C. McCallum, Y. Xu, C.-T. Dinh, J. Li, E. H. Sargent and D. Sinton, *Joule*, 2019, **3**, (11), 2777
53. M. K. Kovalev, H. Ren, M. Z. Muhamad, J. W. Ager and A. A. Lapkin, *ACS Energy Lett.*, 2022, **7**, (2), 599

The Authors

Harry Macpherson completed his Master's in the Carbon Nanomaterials group at the University of Oxford, UK, before developing technology in noble metal alloy processing, lithium-ion battery recycling and CO_2 electrolysis at Johnson Matthey, UK. He is now researching novel approaches to the direct air capture of CO_2 with Deep Science Ventures, UK.

Toby Hodges graduated from the University of York, UK, in 2019 with an MChem in Chemistry, having completed a research project in photochemical CO_2 reduction at the Tokyo Institute of Technology, Japan. His current work as a research scientist at Johnson Matthey focuses on catalyst synthesis for CO_2 electrochemical reduction and electrolyser technologies.

Moyahabo H. Chuma is a research scientist in core capabilities group at Johnson Matthey. Her expertise is in the computational simulation of materials. By making use of modelling techniques, she develops atomic-scale models to investigate physical properties and study chemical reactions. She is interested in heterogeneous catalysis, materials and surface science.

Connor Sherwin is a PhD student in Professor Andrea Russell's group at the University of Southampton, UK. He is currently researching the *operando* X-ray characterisation of gas evolving and consuming electrocatalysts in an industrial collaboration from Johnson Matthey and Diamond Light Source, UK.

Urša Podbevšek is an electrochemist working on development of low-temperature CO_2 reduction systems. She obtained her PhD in Chemical Sciences from University of Ljubljana, Slovenia, focusing on the development of carbon-based electrocatalysts. Her interests include high temperature CO_2 electrolysis, advanced coupled electrochemical techniques and catalyst stability studies.

Katie Rigg graduated from the University of Leeds, UK, in 2018 with a MNatSci in Maths and Chemistry. She is currently working as a researcher at Johnson Matthey specialising in catalyst coated membrane testing for proton exchange membrane water electrolysis, and has also contributed to research in oxygen evolution reaction and CO_2RR catalysis.

Veronica Celorrio is a Beamline Scientist on B18, the core X-ray absorption spectroscopy beamline at Diamond Light Source. Her research interests are the characterisation and understanding of materials with application in electrochemical sciences. She is highly enthusiastic about the opportunities that this research field provides, especially at the interface between materials chemistry and X-ray techniques.

Andrea E. Russell is Professor of Physical Electrochemistry in the School of Chemistry at the University of Southampton. Her research focuses on the discovery and characterisation of electrocatalysts for sustainable energy and chemical production, with emphasis on the use of spectroscopic tools to characterise the catalysts under *operando* conditions. She has collaborated with Johnson Matthey for over 25 years and was a Royal Society Industry Fellow from 2004–2006 at Johnson Matthey.

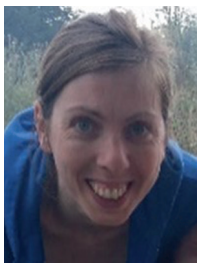

Elena C. Corbos is leading the Electrochemical transformations team at Johnson Matthey. She joined Johnson Matthey in 2010 as a Marie Curie fellow, and has since held several research positions. Her research interests are in materials synthesis with application in sustainable chemicals and fuels production and the development of sustainable technologies to achieve net zero emissions.